NOMAD spectrometer on the ExoMars trace gas orbiter mission: part 2—design, manufacturing, and testing of the ultraviolet and visible channel

Journal Item

applied optics

NOMAD spectrometer on the ExoMars trace gas orbiter mission: part 2—design, manufacturing, and testing of the ultraviolet and visible channel

Manish R. Patel,[1,2,*] Philippe Antoine,[3] Jonathon Mason,[1] Mark Leese,[1] Brijen Hathi,[1] Adam H. Stevens,[1,4] Daniel Dawson,[1] Jason Gow,[1] Timothy Ringrose,[1] James Holmes,[1] Stephen R. Lewis,[1] Didier Beghuin,[3] Philip van Donink,[3] Renaud Ligot,[3] Jean-Luc Dewandel,[3] Daohua Hu,[5] Doug Bates,[5] Richard Cole,[5] Rachel Drummond,[6] Ian R. Thomas,[6] Cédric Depiesse,[6] Eddy Neefs,[6] Eddy Equeter,[6] Bojan Ristic,[6] Sophie Berkenbosch,[6] David Bolsée,[6] Yannick Willame,[6] Ann Carine Vandaele,[6] Stefan Lesschaeve,[7] Lieve De Vos,[7] Nico Van Vooren,[7] Tanguy Thibert,[8] Emmanuel Mazy,[8] Julio Rodriguez-Gomez,[9] Rafael Morales,[9] Gian Paolo Candini,[9] M. Carmen Pastor-Morales,[9] Rosario Sanz,[9] Beatriz Aparicio del Moral,[9] José-Maria Jeronimo-Zafra,[9] Juan Manuel Gómez-López,[9] Gustavo Alonso-Rodrigo,[10] Isabel Pérez-Grande,[10] Javier Cubas,[10] Alejandro M. Gomez-Sanjuan,[10] Fermín Navarro-Medina,[10] Ali BenMoussa,[11] Boris Giordanengo,[11] Samuel Gissot,[11] Giancarlo Bellucci,[12] and Jose Juan Lopez-Moreno[9]

[1]School of Physical Sciences, The Open University, Milton Keynes MK7 6AA, UK
[2]SSTD, STFC Rutherford Appleton Laboratory, Chilton, Oxfordshire OX11 0QX, UK
[3]Lambda-X sa, 102, avenue Schuman, 102, 1401 Nivelles, Belgium
[4]UK Centre for Astrobiology, School of Physics and Astronomy, University of Edinburgh, Edinburgh EH9 3FD, UK
[5]Mullard Space Science Lab, University College London, RH5 6NT, UK
[6]Royal Belgian Institute for Space Aeronomy, BIRA-IASB, Ringlaan 3, 1180 Brussels, Belgium
[7]Optique et Instruments de Précision, Westerring 21, 9700 Oudenaarde, Belgium
[8]Centre Spatial de Liège, Liege Science Park, Avenue du Pre-Aily, 4031 Angleur, Belgium
[9]Instituto de Astrofisica de Andalucia, IAA-CSIC, Glorieta de la Astronomia, 18008 Granada, Spain
[10]Universidad Politécnica de Madrid, IDR/UPM, Plaza Cardenal Cisneros 3, 28040 Madrid, Spain
[11]Royal Observatory of Belgium (ROB) Circular 3, B-1180 Brussels, Belgium
[12]INAF Istituto di Astrofisica e Planetologia Spaziali, Via del Fosso del Cavaliere 100, 00133 Rome, Italy
*Corresponding author: manish.patel@open.ac.uk

Received 23 December 2016; revised 13 February 2017; accepted 15 February 2017; posted 16 February 2017 (Doc. ID 283497); published 24 March 2017

NOMAD is a spectrometer suite on board the ESA/Roscosmos ExoMars Trace Gas Orbiter, which launched in March 2016. NOMAD consists of two infrared channels and one ultraviolet and visible channel, allowing the instrument to perform observations quasi-constantly, by taking nadir measurements at the day- and night-side, and during solar occultations. Here, in part 2 of a linked study, we describe the design, manufacturing, and testing of the ultraviolet and visible spectrometer channel called UVIS. We focus upon the optical design and working principle where two telescopes are coupled to a single grating spectrometer using a selector mechanism.

OCIS codes: (010.4950) Ozone; (120.4570) Optical design of instruments; (120.6085) Space instrumentation; (300.6540) Spectroscopy, ultraviolet.
https://doi.org/10.1364/AO.56.002771

1. INTRODUCTION

The nadir and occultation for Mars discovery (NOMAD) instrument is a three-channel spectrometer suite led by the Belgian Institute for Space Aeronomy (BIRA-IASB), being flown on the ESA/Roscosmos ExoMars Trace Gas Orbiter mission. NOMAD is predominantly based upon the SOIR-channel (solar occultations in the infrared) of the spectroscopy for the investigation of the atmosphere of Venus (SPICAV)

from the highly successful Venus express mission, a compact high-resolution echelle grating spectrometer with acousto-optical tunable filter for the infrared domain between 2.3 and 4.3 μm [1].

NOMAD consists of three separate channels: solar occultation (SO), limb nadir and occultation (LNO), and ultraviolet and visible spectrometer (UVIS), all controlled via a single main electronics interface. SO and LNO are the infrared spectrometers, and are described in the companion paper to this one [2], along with the science aims of the mission and instrument in [3]. The UVIS spectrometer is the subject of this article.

The UVIS channel is a UV/visible spectrometer, capable of observations in both SO and nadir viewing geometries. UVIS is based upon the instrument designed and developed in the UK by the Open University for the ExoMars lander mission as part of the Humboldt payload [4], and adapted for application as an orbital instrument. The UVIS channel is based on a Czerny–Turner layout, a totally different spectrometer concept than the infrared channels. Dual front-end telescopic viewing optics permits two different viewing geometries (SO and nadir) to be achieved with a single spectrometer. Technical details of the UVIS spectrometer are presented here.

2. UVIS DESIGN OBJECTIVES

UVIS was designed to achieve a spectral range of 200–650 nm, with a spectral resolution <2 nm. When measuring in SO mode, its signal-to-noise (SNR) requirement was defined as ≥1000 (230–450 nm) and ≥500 (450–650 nm). In nadir mode the SNR requirement is ≥500 (230–450 nm) and ≥250 (450–650 nm), taking into account all internal noise sources and for a minimum solar signal.

The solar field of view (FoV) of UVIS must be compliant with the general SO objective of attaining a vertical sampling of the atmosphere of at least 1 km. UVIS was therefore designed for a target circular FoV of 2 arcmin, aligned with the FoV of the SO channel. Under the same assumptions as for the LNO channel in nadir mode (400 km above surface, spacecraft speed of 3 km/s, maximum measurement time of 15 s) the footprint of UVIS FoV on the surface of Mars shall not be larger than 60 arcmin by 5 arcmin or 80 km by 5 km. This requirement can be achieved for a circular FoV of the UVIS channel of 43 arcmin. Table 1 gives an overview of the characteristic requirements of the UVIS channel.

A. Instrument Overview

The UVIS instrument is a single spectrometer unit, capable of receiving light from two separate telescopes.

A dual-telescope system feeds a single spectrometer with observed light using a system of optical fibers, coupled to a "selector mechanism." This concept permits two viewing geometries to be achieved using a single spectrometer, significantly reducing the mass required to perform both occultation and nadir measurements (UVIS has a mass of only 950 g).

Light is collected in either the occultation or nadir telescope. It is then fed to the spectrometer via a single optical fiber (occultation) and fiber bundle (nadir) to a selector mechanism, which selects the channel of observation. The light from the selected telescope is then fed into a spectrometer optical bench, where the light is dispersed using diffractive optics. The observed spectrum is then read out from the CCD detector via a set of dedicated electronics.

B. NOMAD and UVIS Design Rules

The general design rules are described in detail in Ref. [2], and are summarized here for ease of reference. ExoMars trace gas orbiter (TGO) is a nadir tracking spacecraft, meaning that its $-y$-axis is always pointing toward and perpendicular to the surface of Mars. NOMAD's three solar lines of sight (one in each of the channels) will be parallel to this limb direction, and hence form an angle of 67.07° with the nadir lines of sight. During SOs the spacecraft adopts an inertial pointing mode, fixed on the center of the Sun, resulting in an apparent ingress or egress of the Sun from the Martian disk.

To fulfil all the NOMAD science goals during SOs, the SO, LNO, and UVIS channels should observe as similar a slice of the atmosphere as possible. To maximize the signal, the SO- and LNO-channel FoV must comprise the entire solar disc and the UVIS-channel FoV must be as central as possible on the Sun. This is so that each of the solar lines of sight is aligned to the instrument's mechanical axis with an accuracy of $\leq \pm 0.15$ mrad. During nadir observations, the footprints of the LNO and UVIS FoV overlap entirely, requiring an alignment accuracy with the mechanical axis of $\leq \pm 10$ mrad. The UVIS-specific requirements are shown in Table 1.

3. TELESCOPE DESIGN

The UVIS channel utilizes a miniature dual-telescope setup to input light into a single spectrometer via optical fibers and a fiber selector mechanism. An overview of the telescope system is shown in Fig. 1.

A. Design Constraints

The constraints imposed on the design of the telescopes are severe when combined. Two observation channels are needed with very different characteristics in terms of transmittance and FoV.

Table 1. UVIS Design Requirements

Characteristic	Value or Range	Unit
General		
Wavelength λ	200–650	nm
Spectral resolution	≤2	nm
Mass	950	g
Dimensions (without periscope)	125 × 165 × 95	mm^3
SO		
Circular FoV	2	arcmin
Vertical sampling	≤1	km
Entrance aperture diameter	20.5	mm
SNR (230–450 nm)	≥1000	
SNR (450–650 nm)	≥500	
Nadir		
Circular FoV	43	arcmin
Entrance aperture diameter	26	mm
Footprint (400 km orbit)	60 × 5	arcmin
	80 × 5	km
SNR (230–450 nm)	≥500	
SNR (450–650 nm)	≥250	

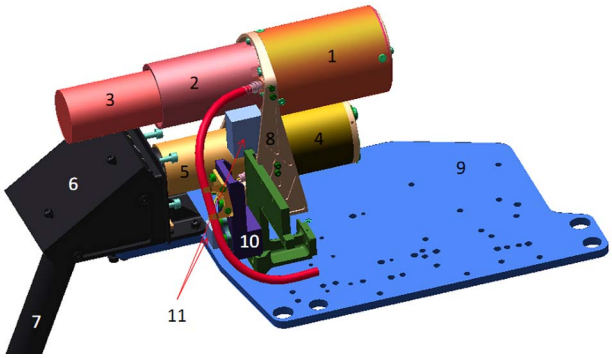

Fig. 1. Telescope overview. (1) Nadir telescope, (2) tube for straylight, (3) nadir light beam, (4) SO telescope, (5) tube for straylight, (6) periscope, (7) occultation light beam, (8) telescope bracket, (9) UVIS baseplate, (10) fiber support mounted on the thermal strap, and (11) alignment cubes.

In the nadir telescope, light is delivered to the spectrometer by a bundle of 19 fibers, each 100 μm in diameter (125 μm including the cladding), as shown in Fig. 2. The diameter of the circumcircle is roughly five times that of a single fiber. Transmittance was required to be as high as possible, since the nadir signal is very low, and the FoV could not exceed 43 arcmin.

In the occultation telescope, the input light must be attenuated by a factor >2000 to avoid saturation (see Section 3.D), in particular when there is no attenuation by the atmosphere. The design is based on the maximum solar radiance assumed to be the spectrum measured by [5] (recorded at minimum solar activity) with a correction factor that estimates the maximum solar activity correction. The FoV was required to be <2 arcmin over the complete spectrum (200–650 nm) to provide a 1 km vertical resolution in the Martian atmosphere.

The overall volume allocated for the telescope system consists of two parallelepipeds whose dimensions are 35 mm × 165 mm × 87 mm and 39 mm × 41 mm × 87 mm. In addition, the telescopes were required to be as light as possible given the overall mass budget for UVIS.

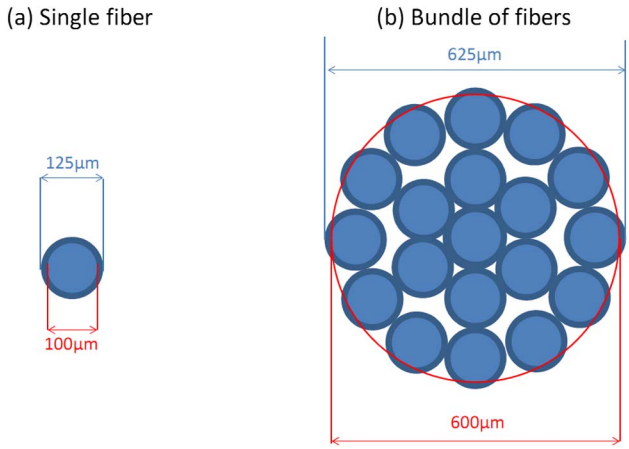

Fig. 2. Fiber configuration for the occultation (left, "Single fiber") and nadir telescopes (right, "Bundle of fibers"). The upper length value defines the resulting core+cladding diameter of the fiber/bundle, and the lower value defines the bare core diameter of the fiber/bundle.

The FoV and the fiber diameter (d) define together the telescope effective focal length (EFL, f):

$$d = 2f \cdot \tan\left(\frac{\text{FOV}}{2}\right). \quad \textbf{(1)}$$

Similarly, the EFL also defines the relation between the telescope input diameter (D) and the numerical aperture (NA) of the fiber:

$$D = 2f\text{NA}. \quad \textbf{(2)}$$

Hence, the main optical characteristics of the telescopes (input beam diameter and EFL) are defined by the UVIS specification, more precisely the FoV, and the choice of the fibers that deliver light to the spectrometer.

B. Reflective Design

Two options were *a priori* possible for the front end optics: refractive or reflective optics. The reflective solution was selected, because it avoids the issue of chromatic aberration. Due to mass and volume constraints, each telescope consists of a single off-axis parabolic mirror. The drawbacks and the advantages of the reflective solution are as follows.

For reflective designs, the system would have to be off-axis. Tilting a spherical mirror would introduce a large level of aberrations to avoid obstruction in the FoV, which could lead to inhomogeneity at the fiber output. Only off-axis parabolic mirrors achieve the necessary focus with a minimum of aberration. This makes the construction and alignment more difficult, and parabolic mirrors are more difficult to polish with high precision.

Using a reflective design is advantageous since the reflectance is, to a large extent, independent of the wavelength. In other words, the FoV is ensured to be exactly the same at each wavelength. The reflectivity (>80%) significantly exceeds the refractive optics transmittance, and degradation due to aging/exposure is minimal.

These advantages largely compensate the manufacturing complexity and motivated the choice of the reflective solution.

C. Nadir Telescope

The telescope of the nadir channel is a single off-axis parabolic mirror with a high-reflection metallic coating. Specifications that define the optical characteristics of the telescope are listed hereafter:

- FoV: 43 arcmin (full FoV)
- Fiber NA: 0.22
- Diameter of the circle that circumscribes the cores of the 19 fibers (see Fig. 2): 625 μm.

The computed parameters are:

- EFL: 46 mm
- Clear aperture (CLAP) diameter: 21.1 mm.

The off-axis distance is 20 mm. The deflection angle is 24.53°. The substrate material is BK7 in order to have the same thermal expansion as the telescope mount, which is made of titanium. An aluminum reflective coating with an MgF_2 protective layer is used to prevent oxidation and provide a

reflectivity of better than 85% over the 200–650 nm spectral range.

Light is collected by a bundle of 19 multimode step-index fibers, as shown previously in Fig. 2. The core diameters of the fiber and of the bundle equal 100 μm and 600 μm, respectively. The fibers are solarization resistant, since they are to be used in the UV range (down to ~200 nm). The coating is in polyimide (hytrel). At the output, the fibers are aligned in a vertical stack in order to maximize the area of coincidence of the fibers and the slit (width = 65 μm).

1. Nadir Mechanical Design

The mechanical design is illustrated in Fig. 3. The three parts of the telescope are mounted on the bracket (not displayed in this figure). Shown are the tube for straylight in pink, the ferrule with its mount, and the main tube of the telescope in orange with the parabolic mirror.

The telescope is made of titanium, to optimize the tensile strength to density ratio and match the thermal expansion to that of BK7. Hence, all the components will expand identically as a function of temperature. FoV, line of sight (LoS) and focusing in the fiber will be to a large extent temperature independent.

The telescope was painted in black with Aeroglaze Z306 black paint. The low outgassing values [total mass loss (TML) = 1.0%, collected volatile condensible material (CVCM) = 0.02%] and high solar absorption (98%) make this paint the optimum choice. A tube connects the periscope and the nadir telescope to prevent straylight from getting in the telescope. The internal surface is texturized to reduce straylight. The tube is made of aluminum and is black anodized.

The fiber is glued in a metallic ferrule that is mounted on the main telescope flange. It is positioned accurately at the focus of the parabolic mirror with multiple screws. The fiber is also tightly maintained in a holder to increase its rigidity (see Fig. 1). The LoS of the nadir telescope is aligned by adjusting the mirror in its mount. Moreover, the fiber has the capability of fine positioning with respect to the focus of the mirror. In the horizontal plane, the fiber and the pinhole can be moved with two screws. In the vertical plane, the fine rotation of the mirror provides the necessary adjustment. The longitudinal position can be tuned with two screws. An offset <5 μm is achievable with the tooling.

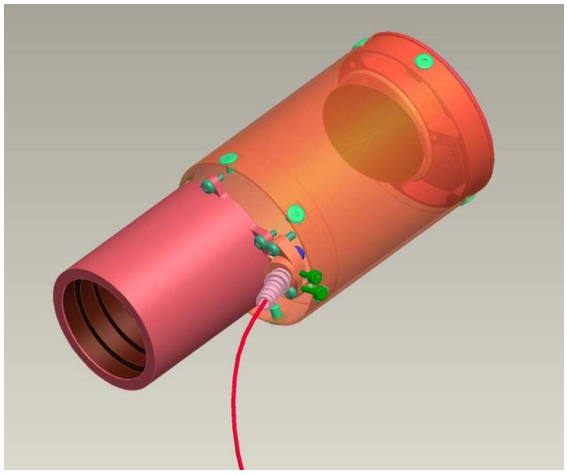

Fig. 3. Mechanical design of the nadir telescope.

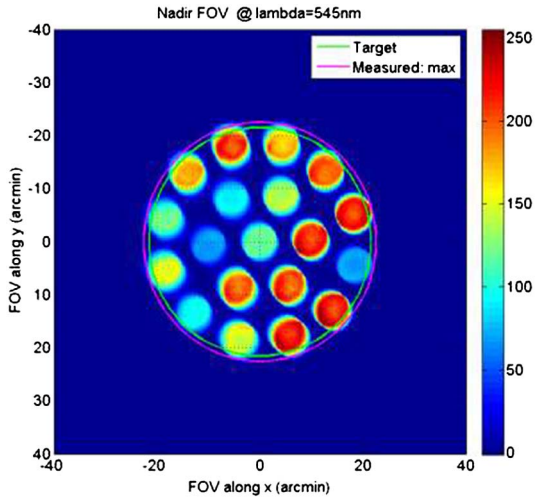

Fig. 4. Nadir FoV measured at 545 nm in arcmin from the center axis. The green circle corresponds to the original FoV requirement. The magenta curve is the measured half-maximum contour line. The color bar is in arbitrary units.

2. Nadir FoV

The FoV of the nadir telescope was defined by using a reversed light path and measuring the angular distribution of light emitted from the telescope input aperture. An example of the measured angular distribution is displayed in Fig. 4 for a wavelength of 545 nm. It is worth noting that the variation in intensity between fibers does not reflect transmittance variations but are due to illumination inhomogeneity of the fibers. The reported FoV (45.2 arcmin) is the maximum measured FoV over all directions. Moreover, the energy encircled inside the target FoV is computed from the 2D distribution, and equals 93.3% of the total energy.

The measured FoV of the nadir telescope over the full spectral range of UVIS ranges between 41.6 and 45.5 arcmin with the energy encircled for each FoV measurement >86%.

D. Occultation Telescope

While the nadir telescope is designed to collect as much signal as possible from the relatively faint surface of Mars, the occultation telescope is designed to look directly at the Sun and therefore observe an object that is much brighter. Attenuation of the signal is the primary objective of this telescope, in order to allow a single spectrometer to successfully sense both the faint nadir signal and also the much stronger SO signal within the dynamic range of the detector (see Section 6).

With respect to the nadir telescope, there are four main differences from the occultation telescope, as illustrated in Fig. 5.

First, a 15 μm pinhole is placed at the tip of the occultation fiber, in order to reduce the collected energy by a factor of 2002/152 = 178. The dimensions of the telescope are scaled down by a factor of 10 with respect to a telescope without pinhole. This would keep the FoV unchanged if the pinhole had a

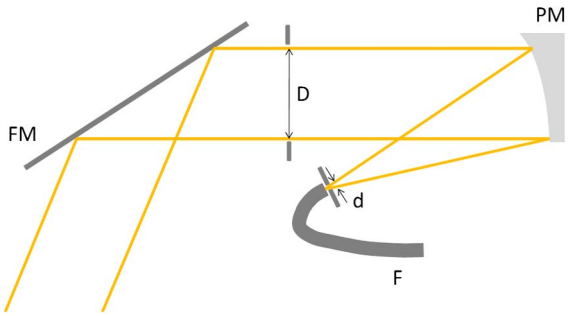

Fig. 5. Layout of the occultation telescope: fiber (F), parabolic mirror (PM), and periscope flat mirror (FM).

diameter of 20 μm. With a 15 μm diameter pinhole, the FoV is narrower. The parabolic mirror is uncoated in order to introduce an additional attenuation of factor ∼20. Use of a neutral density was rejected due to potential aging issues related to the filter substrate that would be used in transmission. Lastly, the mirror in the periscope achieves the fine adjustment of the telescope LoS.

Specifications that define the optical characteristics of the telescope are as follows:

- FoV: 2 arcmin (full FoV)
- Fiber NA: 0.22
- Diameter of the pinhole: 15 μm instead of 20 μm due to mechanical tolerances. This results in a smaller FoV and a smaller signal but is easily compensated for by a longer integration time as needed.

The computed parameters with 15 μm pinhole are:

- EFL: 33.7 mm
- CLAP diameter: 15.7 mm.

The off-axis distance is 13.5 mm. The deflection angle is 22.65°. The substrate material is BK7 to match the thermal expansion with that of the telescope mount, which is manufactured from titanium.

Light is collected by a multimode step-index fiber with a diameter of 200 μm. The fiber is solarization resistant, since it will be used in the UV range (down to 200 nm). The coating is in polyimide (hytrel).

The mirror of the periscope is a flat mirror that only changes the LoS without any impact on the FoV. It is manufactured from BK7 in order to match thermal expansion with the rest of the telescope system. An aluminum reflective coating with an MgF_2 protective layer is used to prevent oxidation. Reflectivity is better than 85% over the 200–650 nm spectral range.

1. Occultation Mechanical Design

The mechanical design is illustrated in Fig. 6. The three parts of the telescope are mounted on the bracket, which is not shown in the figure for clarity.

The telescope mechanical design and materials are the same as those used for the occultation telescope. The edges of the mirror are bonded on three small brackets of the rear flange to minimize stress. The rear flange is designed as an optical trap to minimize straylight, since most of the light power will be transmitted through the uncoated mirror.

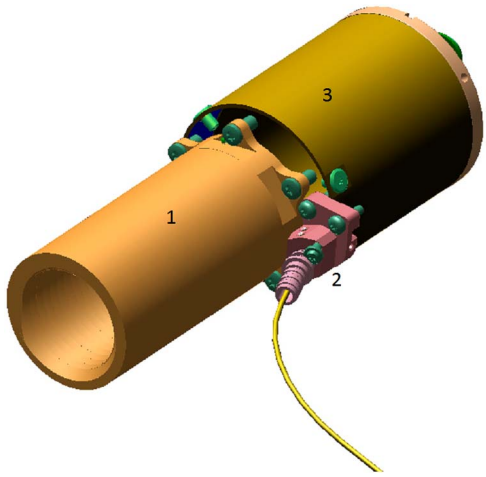

Fig. 6. Structure of the occultation telescope—shown are (1) the tube for straylight, (2) the ferrule and its mount, and (3) the main flange with the parabolic mirror.

A tube connects the periscope and the occultation telescope to prevent straylight from getting in the telescope. The internal surface is textured with small ridges to reduce straylight and is manufactured from aluminum and is black anodized. The optical fiber is glued into a metallic ferrule that is mounted on the main telescope flange. It is accurately positioned at the focus of the parabolic mirror with multiple screws. In the horizontal plane, the fiber and the pinhole can be finely moved with two screws. In the vertical plane, the fine rotation of the mirror provides the necessary adjustment. A 15 μm pinhole is bonded on a holder mounted on the ferrule. The LoS of the occultation telescope is aligned by finely adjusting the mirror in its mount. The pointing alignment accuracy is quite low (1°), since it is determined in reality by the periscope mirror. The fine pointing alignment of the occultation channel was performed with the periscope mirror in order to achieve an instrument-level design accuracy of 0.15 mrad.

2. Occultation FoV

The measured angular distribution is displayed in Fig. 7. The green circle corresponds to the original FoV requirement. The magenta curve shows the measured half-maximum contour line. The reported FoV (1.39 arcmin) is the maximum measured FoV over all directions. Moreover, the energy encircled inside the target FoV is equal to 93%. The direction of elongation of the FoV corresponds to the NOMAD z axis, which is in the plane of the baseplate.

The measured FoV of the occultation telescope over the full spectral range of UVIS varies between 1.38 and 1.68 arcmin with the energy encircled for each FoV measurement >64%.

E. Telescope Bracket

In order to maintain a highly miniaturized design, the two telescopes are mounted on the same titanium bracket. A general view of the bracket is shown in Fig. 8. Its complex design combines rigidity and lightness. The two telescope main flanges, the two straylight tubes, the two fiber holders, and one reference

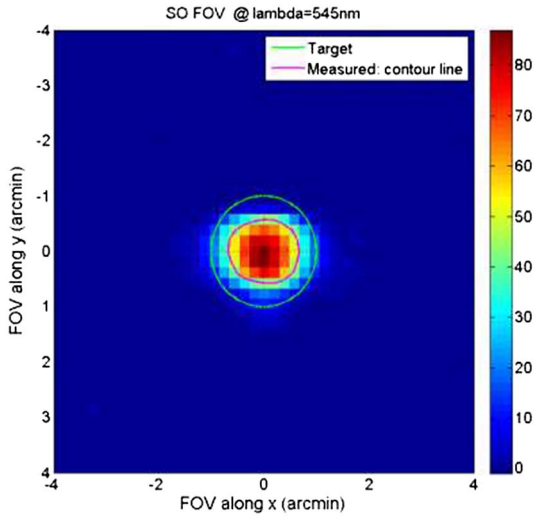

Fig. 7. Occultation FoV measured at 545 nm. The green and the magenta lines correspond to the original requirement and the measured contour line, respectively.

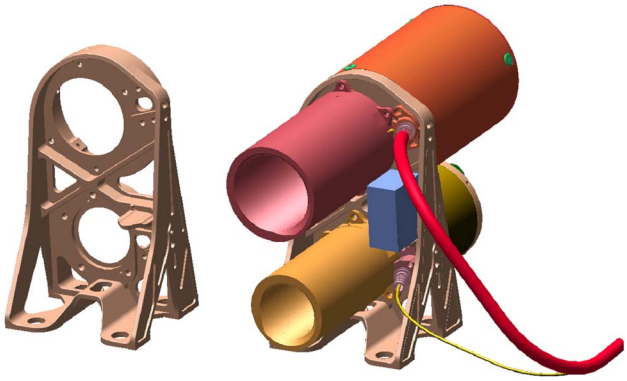

Fig. 8. Overview of the telescope bracket without (left) and with (right) all the parts mounted (two main telescope flanges, two straylight tubes, two fiber holders, and reference cube).

cube are directly mounted on the bracket. The reference cube is glued on the bracket.

The bracket has a mass of 47.5 g. Positioning the bracket is critical, since it determines the telescope LoSs. The bracket alignment is defined by two pins that allow for thermal expansion. They define a fixed location and a fixed direction.

The bracket is fixed on the UVIS baseplate with four screws with spring disks. They achieve an axial force to support the out-of-plane loads while allowing for in-plane sliding of the telescope bracket and the UVIS baseplate separated by spacers in brass.

F. Optical Fiber Assembly

The optical fiber assembly consists of a single optical fiber for the occultation channel, a bundle of 19 fibers for the nadir channel, three ferrules, a fiber holder, and a fiber clamp. The occultation channel requires a single fiber, since the solar intensity is extremely high, whereas the nadir channel (pointed at Mars) has a relatively low signal intensity; hence, higher throughput is required.

The fibers are multimode step-index type fibers with a modified silica core and a doped silica cladding. The core diameter is 200 μm and 100 μm for the occultation fiber and the nadir fibers, respectively. They are solarization resistant and offer a very low attenuation at wavelengths above 190 nm. They are protected by a jacket in hytrel. At one end, the occultation fiber and the nadir fibers are mounted into two stainless steel ferrules. The 19 nadir fibers are inscribed in a circle of 625 μm in diameter. A 2 mm long bore inside the ferrule provides the correct alignment of the fibers with the optical axis.

At the opposite end, the 19 nadir and single SO fibers are mounted in a single ferrule. The nadir fiber bundle and occultation fiber are bonded on the two opposite sides of a spacer in borosilicate glass. As such, the nadir fibers along a vertical line for an optimal overlap with the entrance slit of the spectrometer. The fibers are clamped on a bracket to avoid any force on the selector mechanism due to the bending of the fibers. There is no jacket over the section between the clamp and the common ferrule in order to increase the flexibility of the fiber bundle, which must be moved by the stepper motor.

G. Optical Fiber Selector Mechanism

The selector mechanism, shown in Fig. 9, moves the ferrule containing the occultation and nadir fibers, so that for the relevant observation, the correct fiber(s) is placed in front of the spectrometer slit, thus permitting a single optical bench to observe light from two separate telescopes. The selector mechanism is a copy of the selector mechanism previously approved by European Space Agency (ESA) for the ExoMars Humboldt mission, which was unfortunately cancelled. It consists of three elements: a stepper motor, a gear segment, and a ferrule. The ferrule supports the 19 + 1 fibers and is mounted in the gear segment. The gear segment is supported on a flex pivot, which is in turn held in aluminum housing. The gear rotates on the flex pivot, and it is driven among the three operating positions by a stepper motor. The stepper motor used is the Arsape 1020-V-12-250-01 stepper motor, which has good spaceflight heritage. The motor lubrication is Brayco815Z perfluorinated-based lubricant. The selector positions are: SO fiber, dark, and nadir fiber. The dark position is the default, unpowered position. The other positions are determined by driving against end stops, which can be adjusted to accurately position the fiber.

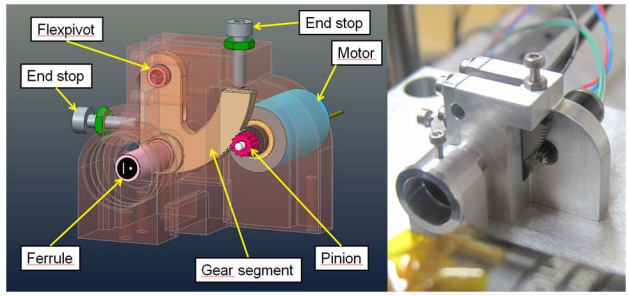

Fig. 9. Layout and concept of the selector mechanism (left) and image of the mechanism (right).

4. SPECTROMETER DESIGN

The spectrometer is based on a Czerny–Turner optical configuration. Figure 10 shows a schematic of the spectrometer layout. Figure 11 is an illustration of the optical layout. The incoming light is delivered by an optical fiber, and the light enters the spectrometer at the slit, passes through an aperture and is focused onto the grating using a primary collimating mirror. The light dispersed by the grating is then focused onto the detector via a secondary collimating mirror. The spectrometer is an imaging system with a magnification equal to 1.

The spectrometer configuration combines simplicity and high performance. In particular, the spectral range is very broad (200–650 nm) with performance optimized for the UV range. Blaze angle and incidence angle achieve the highest reflectance of the first diffraction order at 220 nm (see later sections). Aberrations of the spherical mirrors are smaller in the UV range, and the use of an order-sorting filter solves the issue of the overlap between the first diffraction order and the second diffraction order of the grating.

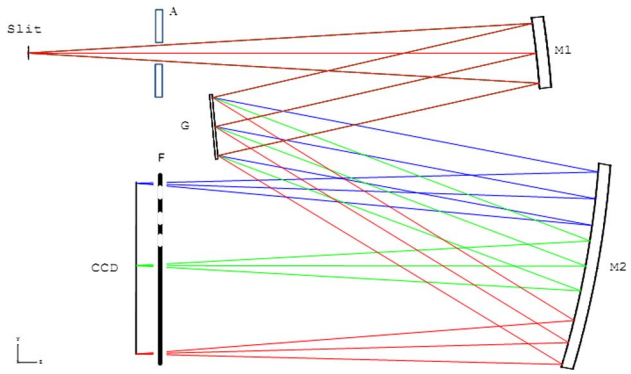

Fig. 10. Optical layout of the spectrometer. The main components, in the order of incoming ray path, are the entrance slit (S), the aperture (A), the collimating mirror (M1), the diffraction grating (G), the focusing mirror (M2), the second-order filter (F), and the detector (CCD). For (F), the dashed line represents the unfiltered part, and the solid line the filtered region.

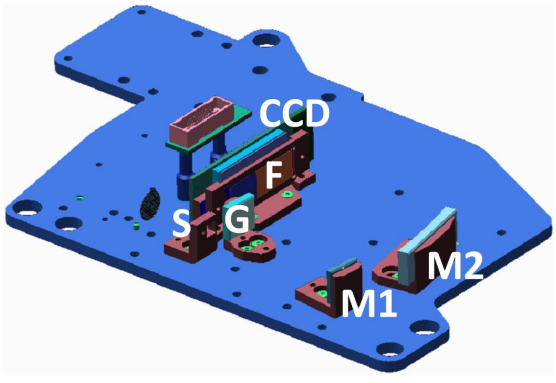

Fig. 11. Layout of the spectrometer optical components on the baseplate: entrance slit (S), the collimating mirror (M1), the diffraction grating (G), the focusing mirror (M2), the second-order filter (F), and the detector (CCD).

A. Structure and Materials

The major structural components of the spectrometer consist of a baseplate and a cover. Both the baseplate and the cover serve dual purposes; the baseplate forms the mechanical interface to the rest of the NOMAD instrument, and also the base upon which the optical components are mounted. The cover suppresses any ambient light, and also incorporates a complex series of baffles and light paths necessary for the dispersive design in such a compact volume.

The baseplate is manufactured from carbon fiber composite to maintain a low mass and high stiffness with minimal thermal expansion. The cover is manufactured from aluminum, and the optical components (described later) are mounted on invar brackets, again to minimize thermal expansion effects, which could lead to misalignment. The reflective optical components (M1, M2, and the grating) are all manufactured by Zerodur, completing the zero thermal expansion design of the spectrometer. All structural surfaces within the spectrometer are painted black using Aeroglaze Z306 (Lord Corporation, U.S.).

B. Slit

The width of the entrance slit is 65 μm, which was determined as a trade-off between spectral resolution (target <1.5 nm) and the SNR of the nadir channel. For use on Mars, SO_2 absorption was chosen as a benchmark for the choice of the width of the slit. Increasing the slit width to 100 μm smooths the SO_2 absorption features to the point that they would not be distinguishable. Any slit between 50 and 75 μm is acceptable, since the SO_2 absorption signature is still visible. Moreover, there is an approximate 25% improvement in the SNR when the slit width is increased from 50 to 75 μm. Hence a slit width of 65 μm results from an optimization of the resolution and the SNR.

C. Spherical Mirrors

The mirrors M1 and M2 (Fig. 10) are spherical mirrors with a focal length of 75 mm. The purpose of these elements is to focus the incident light emerging from the slit onto the detector array.

The mirrors are coated with aluminum with an MgF_2 protective coating to avoid oxidation. They achieve a high reflectance that is, to a large extent, independent of the wavelength. The size of the mirrors and the distance between the entrance slit and M1 defines the NA of the spectrometer. With a mirror of 12 mm height at a distance of 75 mm, the NA of the spectrometer is 0.08, which is lower that of the fiber (0.22). As such, only 13% of the light at the output of the slit is collected by the first spherical mirror.

The spherical shape introduces aberrations (astigmatism, coma) but the aberrations of the two mirrors partially compensate in the tangential plane (dispersion plane). Hence, the spectrometer can achieve a good spectral resolution. In the sagittal plane, the astigmatic aberration elongates the beam, making the size of the beam wavelength dependent. The aberration is noticeable in the (single-fiber) occultation channel but it is not noticeable in the nadir channel (due to the use of multiple stacked fibers). In both these cases, the dispersion in the sagittal plane has no effect on the resulting measurement, since the

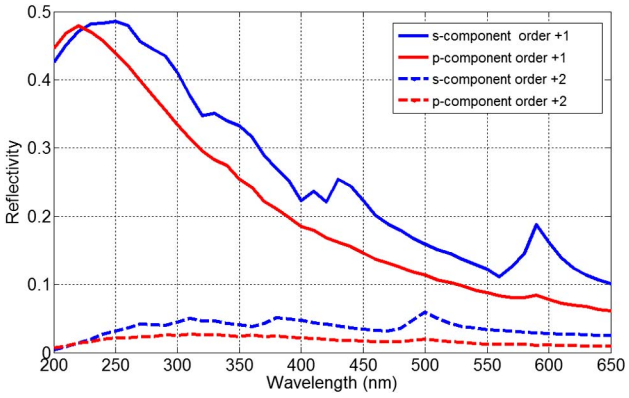

Fig. 12. Reflectance of the grating over the UVIS wavelength range for first and second orders. Reflected order +1 shown in solid lines and order +2 shown in dashed lines.

pixels are binned vertically in the UVIS detector readout process.

D. Grating

Spectral dispersion is performed by a blazed grating that has been optimized for the UV range. The grating is a 12 mm × 12 mm ruled grating (716.418 lines/mm) provided by Newport Corporation, with a blaze angle at 222 nm. The grating has an Al/MgF_2 coating, and the light path from M1 is aligned such that the grating is illuminated very close to the blaze condition. The grating efficiency over the wavelength range is shown in Fig. 12.

The optimized reflectivity in the UV and poor reflectivity at visible wavelengths helps to balance out the relative spectral energy across the spectrum measured at the detector, "equalizing" the measured solar spectrum, which is dominated by visible light. The grating incidence angle is 7.7°, and the diffracted angles at 200 nm, 425 nm, and 650 nm are 16.10°, 26.01°, and 36.85°, respectively.

E. Second-Order Filter

Due to the wide spectral range of the observed signal (200–650 nm), first-diffraction order rays and second-diffraction order rays overlap on the detector. Hence a long-pass filter is used, situated directly in front of the detector in order to block the unwanted second-order rays. It is assumed that the shortest wavelength that corresponds to a significant signal is 160 nm (giving ~40 nm of margin). Hence, the cutoff of the filter is chosen at 325 nm. The filter is a 10 mm × 30 mm window with two "transmission sections."

The first section (covering the short wavelength region of the detector) is an unfiltered region that achieves a transmission coefficient of typically 90% for wavelengths up to 325 nm. The second section (covering the longer wavelength region of the detector) has a coating to block wavelengths below 325 nm and transmit wavelengths above 325 nm (~80% transmission).

A transition area between the two sections, where the edge of the filtered region begins, is unavoidable. This transition region is less than 1 mm long and corresponds to a spectral band width of around 20 nm.

5. ELECTRONICS AND OBSERVATION SEQUENCES

A. Detector

The UVIS detector is an e2 V CCD30-11, which is an advanced inverted mode operation (AIMO) back-illuminated (BI) high performance three-phase buried channel CCD. The detector has an image area of 26.6 mm × 6.7 mm, with an array of 1024 pixels × 256 pixels at a pixel pitch of 26 μm. The CCD used in UVIS was produced using e2v's quantum efficiency (QE) enhanced process with an ultraviolet coating applied to the CCD to increase the QE at short wavelengths. The addition of a boron implant under the integrating electrode defines a fixed potential well when the electrodes are all held at 0 V, which allows charge collection to be performed with the whole surface inverted, minimizing dark current generation and allowing the device to be operated at warmer temperatures.

Three engineering model detectors (from the same batch as the flight) were tested for radiation effects by exposing to 7.5 MeV proton irradiation at the Synergy Health Helios-3 Ion Beam. The dark current, charge transfer inefficiency (CTI), charge storage, and cosmetic quality of the devices were investigated pre- and post-irradiation. In particular, these tests provided information to allow selection of suitable CCD operating voltages for the flight instrument (e.g., substrate voltage, to allow for effect of flatband voltage shift after irradiation), and also demonstrated that the predicted dark current at the expected end of life (EOL) dose would be acceptable.

B. UVIS Electronics System

The UVIS control electronics was designed by the Open University and Mullard Space Science Laboratory (MSSL), UK. The UVIS electronics is designed to perform four main tasks:

(a) provide telemetry and receive telecommands to/from NOMAD;
(b) power, clock, and readout the CCD in various modes and configurations;
(c) drive the optical selector mechanism by controlling a stepper motor;
(d) monitor instrument health by housekeeping (HK) circuits.

C. Front-End Electronics (Detector and Proximity Boards)

The detector board (Fig. 13) hosts the CCD30-11 and its pre-amplifier circuit, which ensures the CCD's raw output is

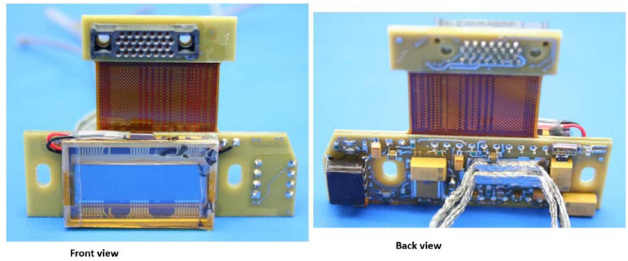

Fig. 13. Flight spare detector board.

amplified as near as possible to the CCD, before any external noise can influence the output. A carefully thought out detector board design and layout improves the SNR and allows the amplified signal to travel further up the chain through the main electronics stack. The back view of the printed circuit board (PCB) (Fig. 13) shows six thermal braids, which thermally connect the PCB to a thermal link to a cool section of NOMAD, helping to keep the CCD within the operating temperature range.

The proximity board hosts all the analog readout circuits. This includes a classic correlated double sampling (CDS) chain, sample-and-hold 16-bit analog-digital converter (ADC), and the CCD clock level shifter and a stepper motor control circuit. The stepper motor circuit is located on this board because it is closest to the optical selector mechanism. The stepper motor is a potential source of noise. Fortunately, the readout is never operated at the same time as stepping the motor, so the noise impact is minimal. Also much attention has been paid in the layout to separate the CDS chain from the CCD clocking and the stepper motor circuits.

D. ReadOut Electronics

The digital board hosts an ACTEL RTAX field-programmable gate array (FPGA), which provides all the telemetry and telecommands (TM/TC) and control of the UVIS channel. The board also hosts all the switching-mode power supplies. Among them, the main DC–DC converter from INTERPOINT provides power isolation between UVIS and SINBAD. The other three small switching converters provide local secondary rails. The reason to have all the switching regulators on the digital board is to keep the switching noise sources as far away from the sensitive analog circuits as possible.

The ACTEL RTAX2000S is based on an antifuse technology and is used as the flight FPGA. This dual-footprint circuit can host either a reprogrammable PROASIC FPGA or a RTAX FPGA. In the debugging stage, the PROASIC was fitted to allow code development and new circuit testing. Only when the design is fully mature and the code frozen was the PROASIC removed and a preprogrammed RTAX chip fitted.

The power board hosts all the other secondary rails, which include five CCD rails, four clocking supplies, and four analog circuit supplies. The CCD rails are sensitive to noise. Any noise coupling into these rails could couple into the CCD output signal, so minimizing the noise levels on these five rails was of highest priority and also the most challenging aspect of the design. The four clocking supplies drive the clocking level shifter. They can also couple into the CCD output mainly through the capacitive coupling paths. Thanks to the periodic operation of these clocks, the noise is not seen when the CCD output is being read out. A clean supply is also vital to ensure the readout electronics introduces minimum noise. As a result, all the secondary rails generated on the power board use linear voltage regulators. Combined with high-quality decoupling capacitors, they can filter most parts of the supply noise over a wide bandwidth.

Three PCBs are interconnected by a 120-way industry standard PC104 connector. This arrangement ensures robust mechanical connection as well as the shortest route for electronics signals travelling between boards.

The CCD can be read out in a full frame or binned column mode depending on operation, with the default science observation mode being vertically binned readouts. Full frame readouts are typically reserved only for calibration activities. The operations are controlled by the FPGA firmware described in the next section.

E. FPGA Firmware

A major function of the firmware is to provide the CCD and CDS clocks, and ADC control to readout the CCD in the various modes required (full frame, region of interest, vertically binned on-chip, and vertically binned off-chip) plus some specific calibration modes. These CCD modes, exposure times, selector mechanism position, and other parameters are determined by interrogating the channel observation parameters (COP) data, which are transmitted to UVIS by NOMAD as part of every operational telecommand (see next section). This method was chosen to allow a fixed determinate firmware while retaining great flexibility in the possible operational routines. The details of these parameters and UVIS operation are discussed in Section 5.F.

F. Observation Sequences and Modes

The science operations during one orbit around Mars can be split in four distinct observations: SO at sunrise terminator; nadir observations at dayside; SO at sunset terminator; and nadir atmospheric emission measurements at the nightside.

To adapt observations of UVIS to these extremely different observation geometries and radiances, UVIS is designed to be programmed in orbit via the COP table, which consists of 512 predefined rows describing various combinations of parameters on how UVIS can be operated. Each individual row of the COP table contains 22 parameters and 24 flags providing flexibility to allow UVIS to be programmed optimally for each observational mode as the mission progresses. The key parameters within the COP table, for any given observation, are described in Table 2.

The spectral data are stored in telemetry packets designated TM(28). For a nominal observation UVIS will transmit one TM(28) packet every 15 s in nadir and three TM(28) packets every second in occultation mode (sub-kilometer vertical resolution). The HK data are stored in telemetry packets designated TM(29) and also embedded in the TM(28) packets. Embedding HK data in the TM(28) provides significant redundancy to ensure that critical HK data are not lost. The COP row values that were used for the observation are also contained in the TM(28) to ensure that, for any observational data, the operational condition of UVIS is always known.

6. OPTICAL AND SPECTRAL PERFORMANCE

A. Spectral Resolution

The spectral resolution of the UVIS spectrometer was determined using an Hg line source for both the nadir and occultation channel. The FWHM of each spectral emission line was measured, and the resulting resolution as a function of wavelength defined. For the occultation channel, the spectral resolution varies between 1.38 and 1.60 nm. For the nadir channel, the spectral resolution varies between 1.20 and 1.53 nm. The difference in spectral resolution is due to the differences in the nadir and occultation telescopes and resulting illumination of the slit by the respective fibers.

Table 2. Key Operational Parameters Contained in the UVIS COP Table

COP Table Parameter	Identifier	Description
Mode	UV-01	Informs UVIS whether the observation is a nadir or occultation
Observation mode	UV-02	Defines whether the observation is a full frame or binned output
Region	UV-06, UV-08 UV-07, UV-09	Four parameters that define the four corners of the region of interest of the CCD pixel array to be read out
Integration time	UV-14	Defines how long the detector is to be exposed to the incident light
Number of acquisitions	UV-15	Has two functions: (1) if "continuous acquisition" flag is "0" then defines how many observations to perform (2) if "continuous acquisition" flag is "1" then defines the number of observations to perform before repeating a dark measurement
Continuous acquisition	UV-21 (bit 2)	Flags to UVIS to either operate continually or to terminate after a defined number of measurements
On/off chip binning	UV-21 (bit 7)	Flags to UVIS whether to accumulate charge in the readout register ("1") or to sum the charge in the FPGA ("0")

B. Telescope Throughput

The throughput of the telescope was measured by comparing the numbers of photons collected by the telescope (N_T) and by a reference system that consists of two pinholes (N_R). The telescope and the reference system were successively illuminated by light emitted by an integrating sphere. The radiance of the emitted light was assumed to be uniform. The count rates with the telescope and the reference system were sufficiently similar to be measured with the same detector and with the same settings. Hence the QE of the detector was the same for the two measurements. The telescope throughput was computed as follows:

$$\text{Throughput} = \frac{N_T}{N_R} \times \text{etendue}. \tag{3}$$

Five different LEDs were used as light sources at 250, 365, 450, 545, and 625 nm. The signal was measured with a photon counting head due to the low emitted flux. Each light source was mounted on one of the ports of the integrating sphere. A fraction of the beam emerging from the integrating sphere was collected successively by the telescope and by the reference system, and the throughput was measured.

The measured etendue for both channels is shown in Fig. 14.

The measured throughput is above the requirement and the throughput is wavelength independent to a large extent. The maximum variation is less than 15%. The most important observation is that the throughput for the occultation channel is below the computed etendue; the opposite case would have indicated a risk of saturation of the detector when the occultation telescope will be illuminated by the Sun.

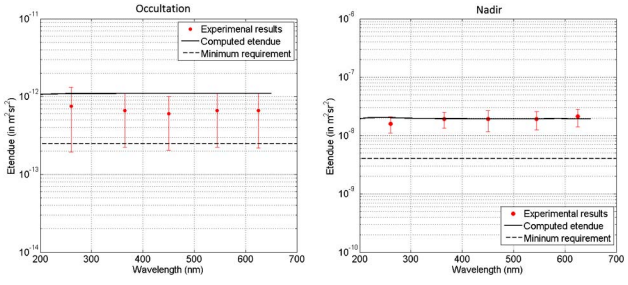

Fig. 14. Etendue of the occultation and nadir telescopes as a function of wavelength. The red dots correspond to the experimental values. The error bars include the uncertainty on the reference system and the repeatability of the measurement. The solid line is the theoretical calculated estimation of the etendue, and the dashed line is the minimum requirement.

C. SNR—Nadir

In nadir, the signal received at the UVIS aperture is the incident solar radiation that is scattered and reflected by Mars. The SNR has been computed for several scenarios [6] considered to be representative of the different conditions that UVIS might observe. They correspond to combinations of the following conditions: two different Sun-Mars distances (aphelion and perihelion); three different albedos (bright spots, dark areas, average), and then either different solar zenith angles or different aerosols loadings.

Due to low incident nadir radiance, the nominal integration time is defined as 15 s. The sources contributing to the noise include: shot noise, dark noise, second-order signal, and thermally generated dark current. Figure 15 shows the magnitude of these noise sources for a worst-case detector temperature of 298 K. It can be seen that in nadir the dominant source of noise is from the thermally generated dark current. Since in nadir long integration times are required, the nadir channel is highly sensitive to the operating thermal environment.

The SNR in nadir observations for different dust loadings to be expected in the Martian atmosphere was computed [6]. The nadir SNR was found to vary by up to 35% due to the variation

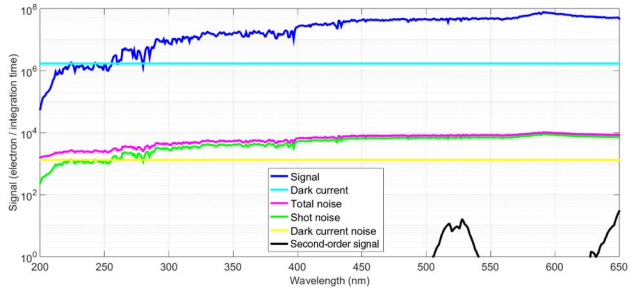

Fig. 15. Signal of the various sources of noise in the UVIS channel. Note: dark current will be subtracted with dedicated observations prior to each measurement. Reproduced from [6].

in atmospheric dust loading, and has a typical value of SNR at UV wavelengths of approximately 500. In all dust conditions considered, the SNR easily reach values above 1000 for wavelengths longer than 300 nm and exceeds 5000 in the visible part of the spectrum.

D. SNR—Occultation

During a SO observation, the incident solar radiance is attenuated by absorption by the Martian atmosphere along the instrument LoS, defined from the center of the Sun to the aperture of the instrument. The reference atmosphere used is based on vertical profiles provided by the GEM-Mars GCM developed at IASB-BIRA [7]. Global annual profiles for the temperature, pressure, CO_2, H_2O, O_3 as well as dust extinction are given from the surface up to 130 km.

Performance of the SO channel has been computed for an integration time of 0.2 s with binning performed over eight CCD rows, as shown in Fig. 16. The operating temperature has been assumed to be a worst-case of 298 K. The impact of the CO_2 absorption at lower wavelengths is clearly seen in Fig. 16, as well as the typical O_3 absorption signature between 220 and 300 nm. Figure 16 (left panel) shows the individual components of the total signal. Unlike nadir, the short integration times and high signal level for the occultation channel result in the occultation system being shot-noise limited. For nominal operating temperatures, and the short integration times required, the thermal dark current is on the order of the readout noise, making the occultation channel insensitive to the detector thermal environment.

The SNR achieved in this configuration (0.2 s integration, binning on eight rows, no spectral binning) is shown in Fig. 16 (right panel). It is also compared with SNR values obtained without any binning, which corresponds to a SNR roughly $\sqrt{8}(\approx 2.8)$ times lower, since the SNR is shot-noise limited. We can clearly see that the SNR follows the radiances, i.e., with the effect of the CO_2 absorption at the lower tangent heights at wavelengths lower than 250 nm as well as the absorption of O_3. SNR > 1000 is easily reached for wavelengths higher than 300 nm. Below this limit, SNR is limited by the attenuation due to the atmosphere itself, mainly CO_2, O_3, and dust aerosols.

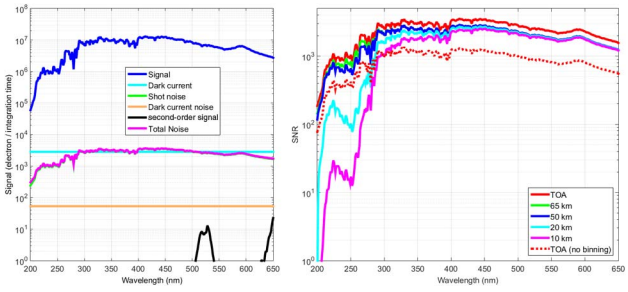

Fig. 16. (Left): signal and noise components for the UVIS SO channel corresponding to an observation at top of the atmosphere (no atmospheric attenuation). (Right): SNR as a function of the wavelength for the UVIS channel operating in SO mode: for an observation at the top of the atmosphere when no binning is considered (dotted red line: SNR for one single line), when binning on eight lines is considered (red line), and for observations corresponding to tangent heights of 65, 50, 20, and 10 km (with binning). Reproduced from [6].

7. CONCLUSIONS

The UVIS channel of NOMAD that is described in this paper will offer good spectral resolution, unprecedented vertical sampling, and excellent sensitivity during SOs and nadir observations of Mars. Building on the heritage development from the ExoMars Humboldt lander, which was subsequently cancelled, UVIS represents a versatile instrument that was successfully adapted from its origins as an *in situ* ground instrument into a remote-sensing instrument.

The reconfiguration of the front-end optics by the addition of two telescopes, transformed the *in situ* spectrometer to make it suitable for orbital deployment. The creative use of an ultra-low mass optical fiber "selector" meant that the two observation geometries of NOMAD (occultation and nadir) could be sensed using a single optical bench, resulting in an ultralight-weight dual-channel spectrometer with a total mass of only 950 g. UVIS therefore represents a new Mars remote-sensing channel of the NOMAD instrument with an extremely high science/mass ratio, providing several years of global mapping and vertical profiles of ozone, dust and aerosols in the Martian atmosphere at the expense of minimal resources. Thus, the NOMAD instrument, which besides the ultraviolet and visible wavelengths also contains two infrared channels (described in the companion paper 2), will deliver new and exciting Martian atmospheric science thanks to a unique combination of spectrometric performances.

Funding. Science and Technology Facilities Council (STFC) (ST/I003061/1, ST/P001262/1, ST/I003096/1, ST/P000886/1); Federaal Wetenschapsbeleid (BELSPO) (4000103401, 4000103402, 4000110796); Ministerio de Ciencia e Innovación (MICINN) (AYA2011-30613-C02-01, AYA2011-30613-C02-02); Ministerio de Economía y Competitividad (MINECO) (AYA2012-39691-C02-01, AYA2012-39691-C02-02); European Commission (EC) (UPWARDS-633127).

Acknowledgment. The NOMAD instrument has been developed under the responsibility of BIRA-IASB, Brussels, with the UVIS channel under the responsibility of the United Kingdom (OU, Milton Keynes) and assisted by BIRA-IASB, Brussels. The industrial lead for UVIS was Lambda-X (Nivelles, Belgium). Associated teams contributing to the design and development of UVIS were OIP (Oudenaarde, Belgium), CSL (Liège, Belgium), IAA-CSIC (Granada, Spain), and IDR-UPM (Madrid, Spain). We thank all engineering and supporting personnel in these teams for their dedicated efforts.

REFERENCES

1. D. Nevejans, E. Neefs, E. Van Ransbeeck, S. Berkenbosch, R. Clairquin, L. De Vos, W. Moelans, S. Glorieux, A. Baeke, O. Korablev, I. Vinogradov, Y. Kalinnikov, B. Bach, J.-P. Dubois, and E. Villard, "Compact high-resolution spaceborne echelle grating spectrometer with acousto-optical tunable filter based order sorting

for the infrared domain from 2.2 to 4.3 μm," Appl. Opt. **45**, 5191–5206 (2006).
2. E. Neefs, A. C. Vandaele, R. Drummond, I. R. Thomas, S. Berkenbosch, R. Clairquin, S. Delanoye, B. Ristic, J. Maes, S. Bonnewijn, G. Pieck, E. Equeter, C. Depiesse, F. Daerden, E. Van Ransbeeck, D. Nevejans, J. Rodriguez-Gómez, J. J. López-Moreno, R. Sanz, R. Morales, and G. P. Candini, "NOMAD spectrometer on the ExoMars trace gas orbiter mission: part 1—design, manufacturing and testing of the infrared channels," App. Opt. **54**, 8494–8520 (2015).
3. "ESA—Robotic exploration of Mars: ExoMars Trace Gas Orbiter," http://exploration.esa.int/mars/46475-trace-gas-orbiter.
4. A. C. Vandaele, E. Neefs, R. Drummond, I. R. Thomas, F. Daerden, J.-J. Lopez-Moreno, J. Rodriguez, M. R. Patel, G. Bellucci, M. Allen, F. Altieri, D. Bolsée, T. Clancy, S. Delanoye, C. Depiesse, E. Cloutis, A. Fedorova, V. Formisano, B. Funke, D. Fussen, A. Geminale, J.-C. Gérard, M. Giuranna, N. Ignatiev, J. Kaminski, O. Karatekin, F. Lefèvre, M. López-Puertas, M. López-Valverde, A. Mahieux, J. McConnell, M. Mumma, L. Neary, E. Renotte, B. Ristic, S. Robert, M. Smith, S. Trokhimovsky, J. Vander Auwera, G. Villanueva, J. Whiteway, V. Wilquet, and M. Wolff, "Science objectives and performances of NOMAD, a spectrometer suite for the ExoMars TGO mission," Planet. Space Sci. **119**, 233–249 (2015).
5. G. Thuillier, M. Herse, D. Labs, T. Foujols, W. Peetermans, D. Gillotay, P. Simon, and H. Mandel, "The solar spectral irradiance from 200 to 2400 nm as measured by the SOLSPEC spectrometer from the ATLAS and EURECA missions," Sol. Phys. **214**, 1–22 (2003).
6. A. Vandaele, Y. Willame, C. Depiesse, I. Thomas, S. Robert, D. Bolsée, M. Patel, J. Mason, M. Leese, S. Lesschaeve, P. Antoine, F. Daerden, S. Delanoye, R. Drummond, E. Neefs, B. Ristic, J. Lopez-Moreno, and G. Bellucci, and Nomad Team, "Optical and radiometric models of the NOMAD instrument part I: the UVIS channel," Opt. Express **23**, 30028–30042 (2015).
7. F. Daerden, J. A. Whiteway, L. Neary, L. Komguem, M. T. Lemmon, N. G. Heavens, B. Cantor, E. Hébrard, and M. D. Smith, "A solar escalator on Mars: self-lifting of dust layers by radiative heating," Geophys. Res. Lett. **42**, 7319–7326 (2015).